ACS APPLIED MATERIALS & INTERFACES

Research Article

www.acsami.org

Surface-Doping Effect of $InVO_4$ Nanoribbons and the Distinctive Behavior as Gas Sensors

Shanshan Liu, Fei Hu, Jie Zhang, Hanxiao Tang, and Mingwang Shao*

Institute of Functional Nano & Soft Materials (FUNSOM), Jiangsu Key Laboratory for Carbon-based Functional Materials and Devices, Soochow University, Suzhou 215123, P. R. China

ABSTRACT: Indium vanadate ($InVO_4$) gas sensors were fabricated by depositing $InVO_4$ nanoribbons aqueous suspension onto ceramic substrates. Their resistances distinctively increased in the detection of ammonia and propylamine, indicating an *n*-to-*p* semiconductor transition. This novel phenomenon of the $InVO_4$-based sensor may be ascribed to the surface doping effect: electrons were trapped by H_2O and O_2 and produced OH^- and O_2^- on the $InVO_4$ surface, which resulted in holes overcompensation in the $InVO_4$ valence band. Moreover, the sufficiently large surface-to-volume ratio of these nanoribbons enables fast carrier transfer on the sensor surface. The $InVO_4$ nanoribbons-based sensors had optimum performance at room temperature and enjoyed good restorability. They also had great response to a wide range of target gas concentration, with ultrahigh sensitivities up to 1100% for ammonia and 760% for propylamine.

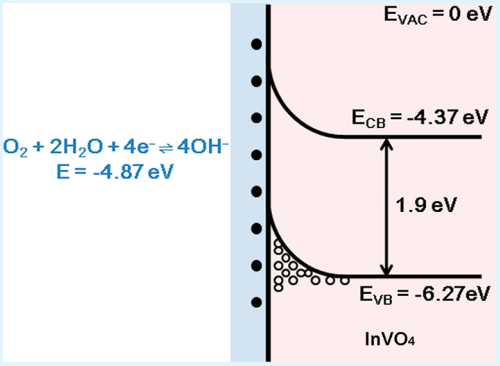

KEYWORDS: *$InVO_4$, nanoribbon, gas sensor, propylamine, ammonia*

INTRODUCTION

Throughout modern industrialization, surface science and technology play an indispensable role in various industrial technologies. Since surface doping theory was applied for hydrogen terminated diamond,[1] hydrogen terminated silicon,[2] carbon nanotubes,[3,4] graphene,[5] and germanium nanowires,[6] it has been widely accepted as a significant surface phenomenon. Surface doping is achieved by chemiadsorption from ambient, and electron exchange between the surface adsorbents and these semiconductors. Meanwhile, absorption and desorption behavior of a gas on the semiconductor oxide surface are extensively investigated, and arouse the use of semiconductor oxides as gas sensors, such as, SnO_2,[7] TiO_2,[8] WO_3, ZnO, In_2O_3,[9] Fe_2O_3, and V_2O_5.[10]

Semiconductor oxide gas sensors have various advantageous features: low cost, high sensitivity, quick response, low detection limit, and long life.[9] In principle, gas sensing by semiconductor oxides is based on the redox reaction with the detected gases occurring on the semiconductor surface, resulting in a change in the resistance of the sensor. Among these semiconductor oxides, one-dimensional (1D) nanostructures, including nanowires, nanotubes, and nanoribbons, are especially suitable for the sensing purposes owing to their large surface-to-volume ratio as well as the consistence in carrier screening length and their lateral scales.[11]

Indium vanadate ($InVO_4$) has commonly been used as anode materials for lithium secondary batteries and photocatalysts[12−14] and electrochemical detection.[15] However, its gas-sensor behavior is barely reported, except in the work of Chen et al., who investigated the sensor behavior of $InVO_4$ particles toward ethanol.[16]

In this work, $InVO_4$ nanoribbons were synthesized by a hydrothermal process. With their width ranging from 50 to 120 nm and their length up to several micrometers, these nanoribbons showed a high aspect ratio and high surface area, which would greatly facilitate the carrier transfer on the material surface. The as-prepared $InVO_4$ was then used for gas sensing toward ammonia (NH_4OH) and propylamine ($C_3H_7NH_2$), both of which are reducing gases and have the same functional group to react with absorbed oxygen. Orthorhombic $InVO_4$ is an *n*-type semiconductor, as reported in other literature.[17,18] When exposed to reducing gases, an *n*-type semiconductor is supposed to show a resistance decrease resulting from increased electrons.[14,19] Whereas it was interesting to find that the resistance of $InVO_4$ distinctively increased upon exposure both to NH_4OH and to $C_3H_7NH_2$, which was explained with the surface doping effect. Moreover, the $InVO_4$ nanoribbon-based sensors showed remarkable sensitivity to NH_4OH and to $C_3H_7NH_2$, giving their gas response range of 20−900 and 10−650 ppm, respectively, at room temperature.

2. MATERIALS AND METHODS

2.1. Preparation of $InVO_4$. $InCl_3{\cdot}4H_2O$, NH_4VO_3, and NH_4OH were purchased from Sinopharm Chemical Reagent Co. Ltd. (Shanghai, China) and used directly without further purification.

The synthesis progress was the same as in our previous work. Typically, 1 mmol $InCl_3{\cdot}4H_2O$ and 1 mmol NH_4VO_3 were added into 35 mL of diluted ammonia solution (pH = 8). After stirring for 30

Received: January 17, 2013
Accepted: March 18, 2013
Published: March 18, 2013

min, the solution was transferred into a 50 mL Teflon-lined autoclave, sealed and maintained at 150 °C for 15 h, and then cooled to room temperature naturally. The precipitate was filtered, washed with distilled water for several times, and then dried under vacuum at 60 °C for 8 h.

2.2. Fabrication of $InVO_4$-Based Gas Sensor. A certain amount of final $InVO_4$ products were dispersed into distilled water and formed into slurry and then coated on ceramic tubelike substrate. The as-fabricated device was dried at 60 °C under vacuum for 24 h.

2.3. Characterization. The as-prepared products were characterized by X-ray diffraction (XRD, a Philips X'pert PRO MPD diffractometer) with Cu Ka radiation (λ = 0.15406 nm). A scanning rate of 0.05° s^{-1} was applied to record the pattern in the 2θ range of 10−70°. The size and morphology of samples were examined by field emission scanning electron microscopy (FESEM, FEI Co., model Quanta-200). The high-resolution transmission electron microscopy (HRTEM) images and transmission electron microscope (TEM) images were taken with HRTEM analyzer (Tecnai G^2 F20).

Gas sensing was conducted using a computer-controlled gas sensing system (WS-30A, Han wei Electronics Co. Ltd., P.R.China). In the measuring electric circuit, a load resistor (10 kΩ) was connected in series with a gas sensor. The circuit voltage was 5 V, and output voltage (V_{out}) was the terminal voltage of the load resistor. A certain amount of NH_4OH or $C_3H_7NH_2$ (Sinopharm Chemical Reagent Co. Ltd.) was injected onto the heating substrate inside the chamber and then evaporated into gas so as to fill the container evenly. The amounts of injected NH_4OH or $C_3H_7NH_2$ were calculated according to their original concentration and the chamber volume (18 L). The gas sensitivity of the sensor in this paper was defined as $S = (R - R_0)/R_0 \times 100\%$, where R and R_0 were the resistance in a test gas and in air, respectively. After the data collection of gas sensitivity, the chamber was blown with air for 5 min, and the target liquid was injected and evaporated for further detection. NH_4OH sensing was measured at 20% RH (relative humidity), and $C_3H_7NH_2$ at 20% RH and 60% RH for comparison.

3. RESULTS AND DISCUSSION

3.1. Characterization of $InVO_4$ Nanoribbons. The powder XRD pattern of the as-prepared products is shown in Figure 1. All the diffraction peaks are consistent with the

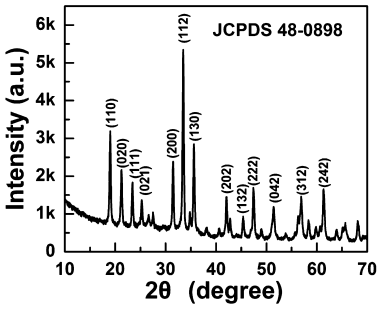

Figure 1. XRD pattern of the as-prepared products showing orthorhombic phase of $InVO_4$.

standard XRD data for the orthorhombic phase of $InVO_4$. The cell parameters of $InVO_4$ are calculated as a = 0.5671 ± 0.0012 nm, b = 0.8395 ± 0.0024 nm, and c = 0.6497 ± 0.0030 nm, which are in good agreement with the standard values (a = 0.573, b = 0.852, and c = 0.6578 nm, JCPDS 48-0898).

Figure 2a and b shows SEM images of a typical $InVO_4$ sample. The layered-structure nature of vanadate favored the formation of one-dimensional products, thus resulted in highly flexible $InVO_4$ nanoribbons as shown in SEM images. There is a single $InVO_4$ nanoribbon with width of 50 nm and thickness of 15 nm calculated from Figure 2c. The cross section of the

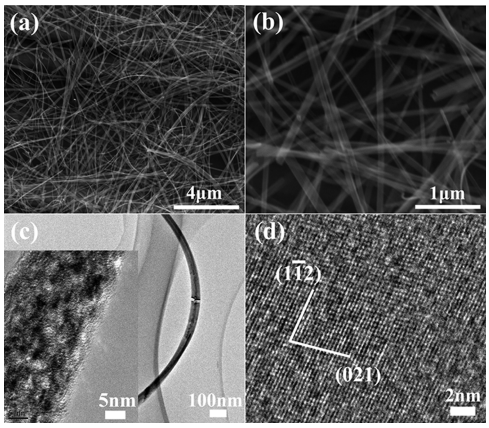

Figure 2. $InVO_4$ nanoribbons: (a, b) SEM images, (c) TEM image, and (d) HRTEM image.

nanoribbon is about 25 nm (inset, Figure 2c), which may be observed from a particular perspective. The HRTEM image (Figure 2d) shows a clear lattice fringe, which manifests the single-crystalline nature of the nanoribbons. The interplanar spacings are measured to be 0.29 and 0.35 nm, which agree well with the lattice spacing of (1−12) and (021) facets of orthorhombic $InVO_4$, respectively.

3.2. Gas Sensing Measurements. Band theory as applied to gas sensors has been the subject of intense study for a number of years.[8,20] When a semiconductor gas sensor is exposed to air, oxygen is adsorbed on the surface of the sensor and go on to trap electrons from the materials conduction band to form species such as O_2^-. As such, in air, the measured resistance of *n*-type semiconductors, whose majority charge carriers are electrons, will increase due to the lower concentration of free electrons in the materials conduction band. On exposure to a reducing gas such as ammonia, surface reaction between the oxygen species and target gas can occur, leading to the release of electrons trapped in the ionized oxygen species back into the materials conduction band, thereby lowering the measured resistance. Likewise, when a *p*-type semiconductor, whose majority charge carriers are positive holes, is exposed to reducing gas, its resistivity increases.[19,21]

Orthorhombic $InVO_4$ is an *n*-type semiconductor.[17,18] However, in our experiments, resistance of $InVO_4$ distinctively increased upon exposure to NH_4OH ambient, demonstrating character of a *p*-type semiconductor.

First of all, gas sensing of $InVO_4$-based devices was performed under different temperatures in order to select an optimum operating temperature (Figure 3). When exposed to 50 ppm NH_4OH or 50 ppm $C_3H_7NH_2$ and then gradually heated, both sensors showed a decline in sensitivities. Thus

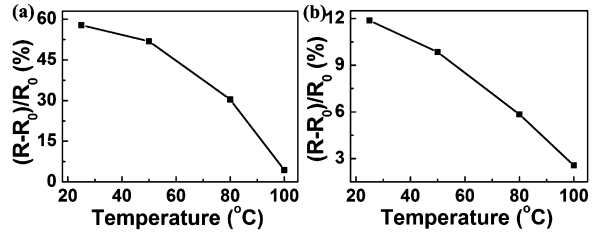

Figure 3. Temperature-dependent responses of $InVO_4$ nanoribbon-based sensors upon exposure to (a) 50 ppm NH_4OH and (b) 50 ppm $C_3H_7NH_2$.

room temperature (~25 °C) was adopted as the optimal operating temperature in all investigations hereinafter.

Then sensitivity changes over increased NH_4OH concentrations were recorded. It is clear from Figure 4a that more gas

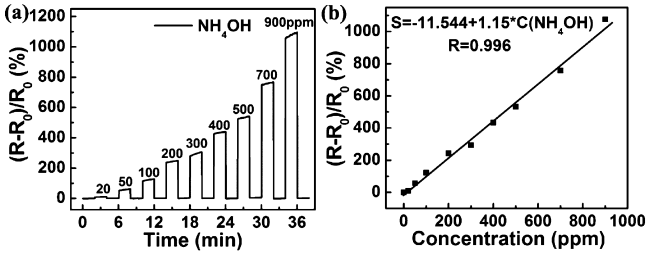

Figure 4. (a) Response of $InVO_4$ nanoribbon-based sensors upon exposure to various concentrations of NH_4OH and (b) linear plot of sensitivity vs the concentration of NH_4OH.

injection leads to higher sensitivity of the sample, which might be ascribed to higher surface coverage and thus more surface reactions taking place.[22] The linear regression equation is S (%) = −11.544 + 1.15C_{amonia} (ppm) in the range from 20 to 900 ppm with a correlation coefficient of 0.996 (Figure 4b). Significantly, the $InVO_4$-based sensor shows fast response rate throughout the sensing measurement, and each time after desorption its resistance gets back to the initial value, showing great recovery performance. ZnO nanowires were used to detect ammonia by Chang et al.[23] The ZnO-based ammonia sensor should be conducted at 300 °C, and the sensitivity only increased from 16% to 36% as ammonia concentration increased from 100 to 1000 ppm. MnO_2 modified ZnO for ammonia sensing was carried out by Patil et al. at room temperature.[24] The MnO_2/ZnO sensor showed a response range of 20−150 ppm, and a maximal sensitivity of 120% when ammonia concentration was 150 ppm. Compared with the above two ZnO-based sensors, the $InVO_4$ nanoribbons-based sensor showed a much wider ammonia response range (20−900 ppm), and a higher sensitivity of 1100%. Moreover, the $InVO_4$ nanoribbons-based sensor is more convenient to use because it has the best sensing performance at room temperature.

From the above findings, we deduce that the large surface-to-volume ratio of nanoribbon structure in part conduces to good sensing. Yet, what exactly breeds the $InVO_4$ n-to-p transition? We therefore propose a mechanism concerning surface band bending: Due to the large number of defects present on the surfaces, adsorption effects are expected to be quite dominant in $InVO_4$ nanoribbon-based sensor. When exposed to air, oxygen and water were adsorbed on $InVO_4$ surface. Oxygen molecules would extract electrons from the conduction band and form O_2^-. As shown in Figure 5, the valence band energy (E_{VB}) and conduction band energy (E_{CB}) of $InVO_4$ are −6.26 and −4.37 eV versus vacuum level. The standard electrode potential of the redox couple $O_2 + 2H_2O + 4e^- = 4OH^-$ is −4.87 eV, so water molecules are able to accept electrons from $InVO_4$. The negative charges on the surface of $InVO_4$ would cause surface band bending, and lead to accumulation of excess holes in the valence band of $InVO_4$. As $InVO_4$ is an n-type semiconductor, excess holes from surface adsorption should have been enough to fully compensate the electrons in nanoribbons, and enable $InVO_4$ surface to display p-type character.[25−27]

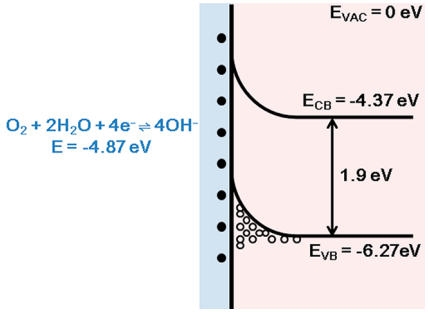

Figure 5. Schematic of energy band of $InVO_4$ in air. CB, VB, and VAC are conduction band, valence band, and vacuum level, respectively. The solid dots represent O_2^- and OH^- ions, and the hollow ones denote holes.

To corroborate this point, sensing measurements for $C_3H_7NH_2$ at different relative humidities were carried out. $C_3H_7NH_2$ was first detected at 60% RH air (Figure 6a and b); a

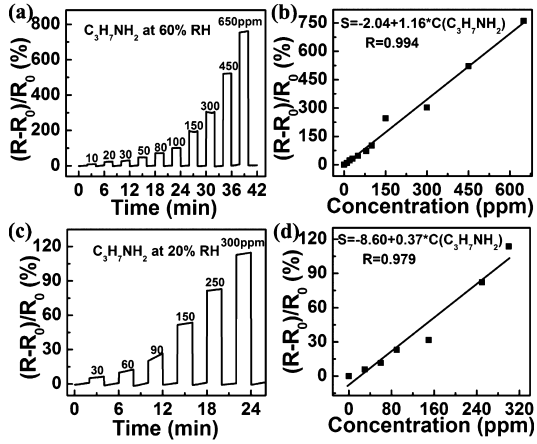

Figure 6. (a, c):Response of $InVO_4$ nanoribbon-based sensors upon exposure to various concentrations of $C_3H_7NH_2$ at 60% RH and 20% RH, respectively. (b, d) Linear plot of sensitivity vs the concentration of $C_3H_7NH_2$ at 60% RH and 20% RH.

linear dependence between gas concentration (10−650 ppm) and sensitivity is observed. The linear equation is fitted to be S = −2.04 + 1.16$C_{(propylamine)}$, and the correlation coefficient R to be 0.994. In the linear interval, the sensitivity reaches a highest value of 760% when the gas concentration is 650 ppm, revealing remarkable sensing performance of the $InVO_4$ nanoribbon-based sensor. However, in a low relative humidity (20% RH), the result is quite different, as shown in Figure 6c and d. The linear range is relatively narrow (30−300 ppm), which is determined to be S = −8.60 + 0.37$C_{(propylamine)}$ with the correlation coefficient R of 0.994. Its sensitivity is much less than that at 60% RH. Moreover, in the initial stage, the sensor shows lower sensitivities at 20% RH than that at 60% RH, 82% at 250 ppm, versus 101% at 100 ppm. The explanations may be as follows: in an ambient with low relative humidity, less H_2O was adsorbed onto the sensor surface, causing less holes accumulation in $InVO_4$ valence band and thus a smaller resistance increase upon exposure to reducing gas.

4. CONCLUSIONS

In summary, $InVO_4$ nanoribbons-based gas sensors were fabricated by coating $InVO_4$ aqueous suspension onto ceramic

substrates. Significantly, when applying these sensors to NH_4OH and $C_3H_7NH_2$ monitoring, an *n*-to-*p* semiconductor transition was observed. This might be rationalized by excess holes accumulation in $InVO_4$ valence band, which was resulted from electron trapping by surface absorbed water and oxygen molecules. In addition, the high aspect ratio and large specific area of $InVO_4$ nanoribbons greatly facilitated carrier transfer on the sensor surface, which partially conduced to the extremely high sensitivities toward NH_4OH (1100%) and $C_3H_7NH_2$ (760%) sensing. Furthermore, these sensors possessed wide gas response range, low operating temperature, and good recovery performance. Taken together, these features make $InVO_4$ nanoribbons well suited for applications in gas sensors.

AUTHOR INFORMATION

Corresponding Author

*E-mail: mwshao@suda.edu.cn. Fax: +86 512 65882846. Tel: +86 512 65880953.

Notes

The authors declare no competing financial interest.

ACKNOWLEDGMENTS

The financial supports from Natural Science Foundation of China (No. 21071106), the National Basic Research Program of China (973 Program) (No. 2012CB932900), and Specialized Research Fund for the Doctoral Program of Higher Education (20103201110016) are acknowledged.

REFERENCES

(1) Strobel, P.; Riedel, M.; Ristein, J.; Ley, L. *Nature* **2004**, *430*, 439−441.
(2) Fuechsle, M.; Miwa, J. A.; Mahapatra, S.; Ryu, H.; Lee, S.; Warschkow, O.; Hollenberg, L. C. L.; Klimeck, G.; Simmons, M. Y. *Nat. Nanotechnol.* **2012**, *7*, 242−246.
(3) Collins, P.; Bradley, K.; Ishigami, M.; Zettl, A. *Science* **2000**, *287*, 1801 −1804.
(4) Kong, J.; Franklin, N. R.; Zhou, C.; Chapline, M. G.; Peng, S.; Cho, K.; Dai, H. *Science* **2000**, *287*, 622−625.
(5) Chen, W.; Chen, S.; Qi, D. C.; Gao, X. Y.; Wee, A. T. S. *J. Am. Chem. Soc.* **2007**, *129*, 10418−10422.
(6) Luo, L. B.; Yang, X. B.; Liang, F. X.; Jie, J. S.; Wu, C. Y.; Wang, L.; Yu, Y. Q.; Zhu, Z. F. *J. Phys. Chem. C* **2011**, *115*, 24293−24299.
(7) Chen, D.; Xu, J.; Xie, Z.; Shen, G. Z. *ACS Appl. Mater. Interfaces* **2011**, *3*, 2112 −2117.
(8) Fine, G. F.; Cavanagh, L. M.; Afonja, A.; Binions, R. *Sensors* **2010**, *10*, 5469−5502.
(9) Kanan, S. M.; El-Kadri, O. M.; Abu-Yousef, I. A.; Kanan, M. C. *Sensors* **2009**, *9*, 8158−8196.
(10) Comini, E. *Anal. Chim. Acta* **2006**, *568*, 28−40.
(11) Choi, K. J.; Jang, H. W. *Sensors* **2010**, *10*, 4083−4099.
(12) Orel, B.; Vuk, A. S.; Krasovec, U. O.; Drazic, G. *Electrochim. Acta* **2001**, *46*, 2059−2068.
(13) Vuk, A. S.; Krasovec, U. O.; Orel, B.; Colomban, P. *J. Electrochem. Soc.* **2001**, *148*, H49−H60.
(14) Ye, J.; Zou, Z.; Oshikiri, M.; Matsushita, A.; Shimoda, M.; Imai, M.; Shishido, T. *Chem. Phys. Lett.* **2002**, *356*, 221−226.
(15) Liu, S. S; Shao, M. W.; Liao, F. *CrystEngComm* **2012**, *14*, 3441−3445.
(16) Chen, L. M.; Liu, Y. N.; Lu, Z. G.; Zeng, D. M. *J. Colloid Interface Sci.* **2006**, *295*, 440−444.
(17) Butcher, D. P., Jr.; Gewirth, A. A. *Chem. Mater.* **2010**, *22*, 2555−2562.
(18) Enache, C. S.; Lloyd, D.; Damen, M. R.; Schoonman, J. *J. Phys. Chem. C* **2009**, *113*, 19351−19360.
(19) Elouali, S.; Bloor, L. G.; Binions, R.; Parkin, I. P.; Carmalt, C. J.; Darr, J. A. *Langmuir* **2012**, *28*, 1879−1885.
(20) Li, Y. S.; Xu, J.; Chao, J. F.; Chen, D. *J. Mater. Chem.* **2011**, *21*, 12852−12857.
(21) Barsan, N.; Weimar, U. *J. Electroceram.* **2001**, *7*, 143−167.
(22) Tan, O. K.; Zhu, W.; Yan, Q.; Kong, L. B. *Sens. Actuators, B* **2000**, *65*, 361−365.
(23) Chang, S. J.; Weng, W. Y.; Hsueh, T. J. *Nano Commun Netw* **2010**, *1*, 283−288.
(24) Patil, L. A.; Sonawane, L. S.; Patil, D. G. *J. Mod. Phys.* **2011**, *2*, 1215−1221.
(25) Jie, J. S.; Zhang, W. J.; Peng, K. Q.; Yuan, G. D.; Lee, C. S.; Lee, S. T. *Adv. Funct. Mater.* **2008**, *18*, 3251−3257.
(26) Kirihara, K.; Kawaguchi, K.; Shimizu, Y.; Sasaki, T.; Koshizaki, N. *Appl. Phys. Lett.* **2006**, *89*, 243121−243123.
(27) Williams, D. E.; Moseley, P. T. *J. Mater. Chem.* **1991**, *1*, 809−814.